Resources, Conservation & Recycling 180 (2022) 106209

Contents lists available at ScienceDirect

Resources, Conservation & Recycling

journal homepage: www.elsevier.com/locate/resconrec

Regenerable solvents mediate accelerated low temperature CO_2 capture and carbon mineralization of ash and nano-scale calcium carbonate formation

Tianhe Yin [a], Shufan Yin [a], Akanksha Srivastava [a], Greeshma Gadikota [a,b,*]

[a] School of Civil and Environmental Engineering, Cornell University, Ithaca, NY 14853, USA
[b] Smith School of Chemical and Biological Engineering, Cornell University, Ithaca, NY 14853, USA

ARTICLE INFO

Keywords:
Carbon mineralization
CO_2 capture solvents
Fly ash and waste ash
Calcium carbonate

ABSTRACT

The dual need to remove CO_2 from our emissions and treat alkaline industrial residues such as ash materials motivate the design of innovative pathways to simultaneously capture and convert CO_2 into mineralized carbonates. Direct carbon mineralization is one approach that addresses the need to simultaneously treat alkaline industrial residues and mineralize CO_2 emissions. Low CO_2 solubility in water and slow kinetics at ambient temperature have challenged the direct carbon mineralization of alkaline industrial residues. To address these challenges, the use of CO_2 capture solvents that enhance CO_2 solubility and facilitate accelerated carbon mineralization of fly ash at temperatures below 90 °C is investigated. Calcium carbonate formation results in the inherent regeneration of the solvent. The carbon mineralization extents of non-calcium carbonate content in fly ash were 50% and 51% and in waste ash were 58% and 62% in 2.5 M sodium glycinate and 30 wt% MEA solutions, respectively. The experiments were performed at 50 °C for 3 h with CO_2 partial pressure of 1 atm in a continuously stirred slurry environment with 15 wt.% solid. Furthermore, nanoscale $CaCO_3$ is successfully synthesized from dissolved calcium using CO_2-loaded sodium glycinate and surfactants such as CTAB (Cetyl Trimethyl Ammonium Bromide). Surfactants such as CTAB bind to the calcium carbonate surface and regulate the growth of calcium carbonate particles. These innovative approaches demonstrate the feasibility of directly storing CO_2 in fly ash and waste ash as calcium carbonate and producing nanoscale calcium carbonate using regenerable CO_2 capture solvents.

1. Introduction

Energy efficient strategies to remove CO_2 from our air and emissions while harnessing abundant low value alkaline resources are crucial for a sustainable climate and environmental future. Thermodynamically downhill carbon mineralization routes which involve converting CO_2 into inorganic carbonates are emerging as sustainable approaches to remove CO_2 from our emissions and air by utilizing earth abundant industrial residues and natural mineral resources (Chang et al., 2011b; Ding et al., 2014; Gadikota et al., 2014; Huijgen et al., 2006, 2005; Huntzinger et al., 2009; Ji et al., 2019; Montes-Hernandez et al., 2009; Yadav et al., 2010; Yan et al., 2013). In addition, carbon mineralization routes could also be utilized to harness various types of industrial residues for producing wide ranging products such as Si-rich residues, precipitates enriched in Fe and Cr, or high-purity precipitated calcium carbonate (Höllen et al., 2018). To accelerate carbon mineralization behavior, various research efforts have focused on enhancing the dissolution behavior of silicates and alumino-silicates using strong and weak acids (Benhelal et al., 2021; Wolff-Boenisch et al., 2011) and chelating agents that bind the Ca^{2+} or Mg^{2+} ions to enhance ion solvation (Bobicki et al., 2014; Declercq et al., 2013; Wang et al., 2021). Further, carbonate precipitation is aided at elevated pH conditions and by using seeding surfaces (Donnet et al., 2005; Korchef and Touaibi, 2020; Mercer et al., 2005). Despite these advances, enhancing the solubility of CO_2 for accelerated carbon mineralization has been a long-standing scientific challenge. Biomimetic catalysts such as carbonic anhydrase have been developed to enhance CO_2 solubility (Di Lorenzo et al., 2018; Russo et al., 2013; Verma et al., 2021). However, these materials are sensitive to elevated temperatures where carbon mineralization is often accelerated (Migliardini et al., 2014; Verma et al.,

* Corresponding author at: School of Civil and Environmental Engineering, Cornell University, Ithaca, NY 14853, USA.
E-mail address: gg464@cornell.edu (G. Gadikota).

https://doi.org/10.1016/j.resconrec.2022.106209
Received 25 November 2021; Received in revised form 20 January 2022; Accepted 27 January 2022
Available online 5 February 2022

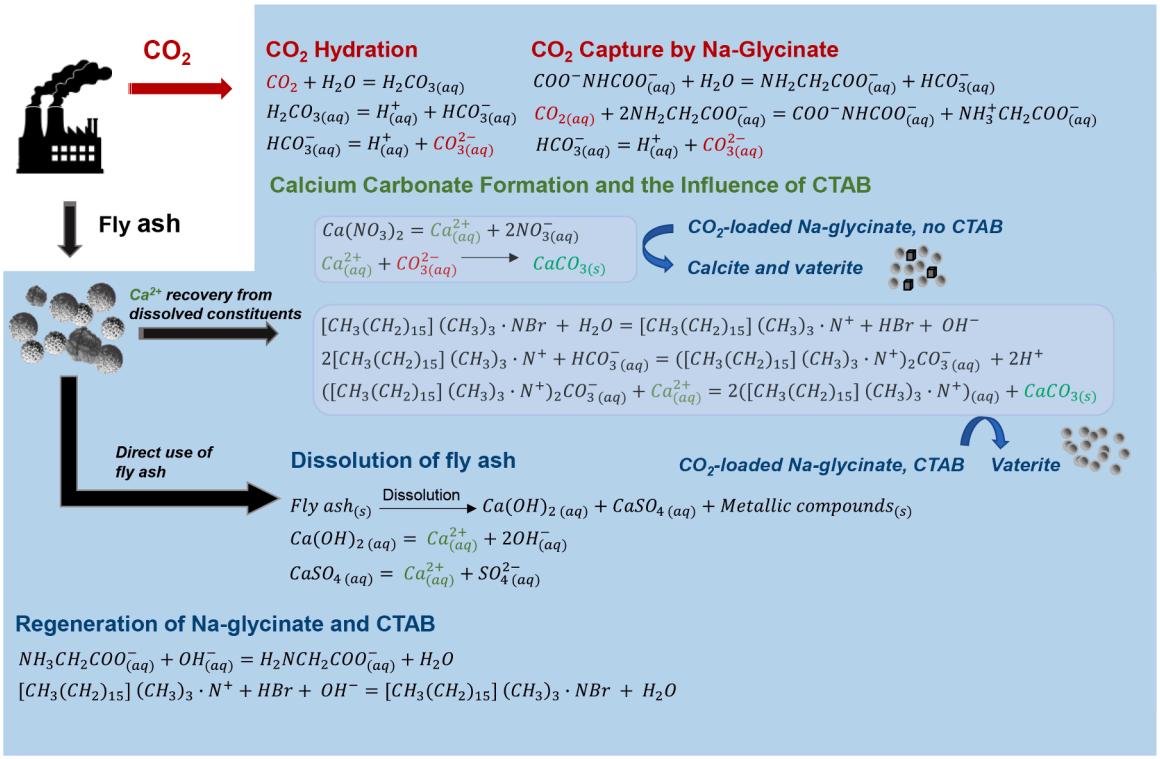

Fig. 1. Schematic representation of integrated CO_2 capture and carbon mineralization using sodium glycinate as a regenerable solvent and CTAB to suppress the size of calcium carbonate particles.

2021). Therefore, alternative approaches to enhance CO_2 solubility while synergistically aiding carbon mineralization at temperatures below 90 °C need to be developed.

One emerging approach to enhance CO_2 solubility while accelerating carbon mineralization involves the use of regenerable solvents. Recent efforts have shown that amine bearing solvents for capturing CO_2 can be chemically regenerated via calcium carbonate formation (Hong et al., 2020; Liu et al., 2021; Liu and Gadikota, 2020, 2019; Yu et al., 2019). The alkalinity sources for these studies ranged from high purity solutions bearing calcium (Hong et al., 2020) to pure precursor calcium oxide, magnesium oxide, and calcium silicate (Liu et al., 2021; Liu and Gadikota, 2020, 2019). Pure precursor calcium and magnesium-bearing minerals were investigated to develop calibrated insights into carbon mineralization using regenerable solvents. However, the efficacy of using heterogeneous materials such as ash samples for integrated CO_2 capture and carbon mineralization with inherent solvent regeneration has not been investigated. This approach is a significant departure from the use of elevated temperature and high purity CO_2 partial pressure to accelerate carbon mineralization (Gadikota et al., 2014; Gerdemann et al., 2003; Huijgen et al., 2006; Wang et al., 2019) or the use of acids to dissolve the mineral followed by using basic solutions to achieve carbonate formation at elevated pH conditions (Azdarpour et al., 2015, Azdarpour et al., 2014; Kodama et al., 2008; Wang and Maroto-Valer, 2011). These strategies have been successfully demonstrated with naturally occurring calcium or magnesium-bearing silicate minerals (Babiker and Ahlstrand, 2019; Daval et al., 2009a; Di Lorenzo et al., 2018; Gadikota et al., 2014; Harrison et al., 2013; Huijgen et al., 2006; Min et al., 2017; Tai et al., 2006; Wang et al., 2019; Yan et al., 2013) and heterogeneous alkaline residues such as fly ash (Bauer et al., 2011; Li et al., 2007; Montes-Hernandez et al., 2009; Nyambura et al., 2011; Uliasz-Bocheńczyk et al., 2009; Wang et al., 2008), cement kiln dust (Huntzinger et al., 2009; Anderson, 2006), paper mill waste (Pérez-López et al., 2008), steel slags (Baciocchi et al., 2009; Bonenfant et al., 2008; Chang et al., 2012, 2011b, 2011a; Eloneva et al., 2008; Huijgen et al., 2005; Kodama et al., 2008), and red mud (Yadav et al., 2010).

Integrated CO_2 capture and carbon mineralization pathways overcomes the challenge of low solubility of CO_2 in aqueous environments by using CO_2 capture solvents that concentrate carbonate and bicarbonate species in the aqueous phase. Reactions of CO_2-bearing solvents with calcium- or magnesium-bearing fluids or solids result in the formation of the corresponding carbonates and the inherent regeneration of the solvents. The effectiveness of solvents such as monoethanolamine (MEA) (Hong et al., 2020; Liu and Gadikota, 2019; Sanna et al., 2014), diethanolamine (DEA) (Hong et al., 2020), methyl diethanolamine (MDEA) (Hong et al., 2020), 2-amino-2-methyl-1-propanol (AMP) (Hong et al., 2020; Liu et al., 2021), 1,8-Diazabicyclo[5.4.0]undec-7-ene (DBU) (Liu et al., 2021), and sodium glycinate (Na-glycinate) (Liu and Gadikota, 2020) on accelerating carbon mineralization with respect to the base case (i.e. using water alone without the solvent) was investigated. These studies revealed that MEA and sodium glycinate are effective in enhancing carbon mineralization, which is attributed to fast CO_2 capture kinetics and the ease of solvent regeneration. Sodium glycinate is preferred since it is more chemically stable, environmentally benign and less corrosive compared to monoethanolamine. However, gel-like mass transfer limiting phases are noted when AMP or DBU solvents are used in the presence of calcium silicate, which limits carbon mineralization (Liu et al., 2021).

Another key consideration is the regeneration of the solvent for effective and economical use over multiple cycles. Prior studies with pure precursors such as CaO, $CaSiO_3$, and MgO revealed that temperatures in the range of 25–90 °C are effective in enhancing CO_2 capture and mineralization with inherent solvent regeneration (Liu et al., 2020; Liu and Gadikota, 2020, 2019). Typically, lower temperatures favor CO_2 capture via absorption and higher temperatures favor dissolution of alkaline substrates and carbonate formation. Prior studies have shown that temperatures of 50 and 75 °C aid the mineralization of CaO, MgO and $CaSiO_3$ (Liu et al., 2020; Liu and Gadikota, 2020, 2019).

Among alkaline industrial residues, ash samples generated from power plants (Chen et al., 2018) has significant potential for storing CO_2

Table 1
Compositions of fly ash and waste ash based on X-Ray Fluorescence (XRF) analyses.

Component	Fly ash (wt.%)	Waste ash (wt.%)
CaO	37.40	35.90
MgO	4.15	4.05
Fe_2O_3	3.77	3.99
Al_2O_3	10.00	10.00
SiO_2	17.80	18.80
Na_2O	1.68	1.56
K_2O	0.20	0.20
TiO_2	0.67	0.69
P_2O_5	0.59	0.53
MnO	0.04	0.04
Cr_2O_3	< 0.01	< 0.01
V_2O_5	0.02	0.02
LOI[a]	8.56	10.5

[a] LOI: loss of Ignition.

as inorganic carbonates due to the large quantities generated. For example, approximately 750 million tons of fly ash was generated in 2015 (Gollakota et al., 2019; Yao et al., 2015). In addition to producing Ca- and Mg-carbonates, carbon mineralization can immobilize heavy metals (Wu, 2017). It has been reported that carbon mineralization effectively reduced the leaching of heavy metals from ladle furnace slag (LFS), especially for Pb and Zn (Xu and Yi, 2022). Aqueous hydrothermal routes were found to be more effective in aiding carbon mineralization compared to direct gas-solid reactions. Enhanced dissolution, mass transfer and reactivity of ions in aqueous hydrothermal environments aid accelerated carbon mineralization. However, the reported extents of carbon mineralization of fly ash vary significantly in literature, as the calcium oxide content can vary from less than 5% (Montes-Hernandez et al., 2009) to more than 50% (Wang et al., 2008) which can impact the reaction efficiency.

One of the less explored approaches to valorize alkaline industrial residues such as fly ash involves synthesizing nano-scale calcium carbonate, which is of higher value compared to the carbonate-bearing product produced directly from fly ash. Nano-scale calcium carbonates have wide-ranging applications in paper, rubber and paint industries (Barhoum et al., 2014; El-Sheikh et al., 2013; Lei et al., 2006). One approach to suppress the growth of calcium carbonate into larger particles is by using surfactants such as cetyltrimethylammonium bromide (CTAB). CTAB molecules bind to the nucleating calcium carbonate surfaces and prevent further growth (El-Sheikh et al., 2013). However, the feasibility of producing nanoscale calcium carbonate from dilute CO_2-bearing flue gas streams using CTAB and regenerable solvents has not been explored. This approach has a high transformative potential since CO_2-bearing flue gas streams and regenerable solvents are directly used to produce nano-scale calcium carbonate from ash materials as an alternative to energy-intensive mechanical grinding approaches to produce nano-scale calcium carbonate.

In this study, we elucidate the reactivity of ash materials using an integrated CO_2 capture and carbon mineralization approach with inherent solvent regeneration and explore the feasibility of limiting the particle growth of micrometer-sized calcium carbonate to produce nanoscale particles. Fly ash and waste ash (which is a mixture of fly ash and bottom ash) were selected as representative ash materials generated during coal combustion. The influence of two solvents for CO_2 capture and carbon mineralization, sodium glycinate and monoethanolamine (MEA) at 50 ℃, CO_2 partial pressure of 1 atm, solid weight of 15%, and a stirring rate of 300 rpm for a reaction time of 3 h is investigated. The base case involves the use of water as an alternative to the use of solvents. We demonstrate the feasibility of producing nanoscale calcium carbonate directly using gaseous CO_2 and calcium nitrate solution by harnessing sodium glycinate to capture CO_2 and CTAB to modulate the sizes of calcium carbonate. These studies demonstrate approaches to co-utilize fly ash and waste ash and CO_2 for direct CO_2 capture and carbon mineralization and to produce nanoscale calcium carbonate using chemically regenerable solvents (Fig. 1).

2. Materials and methods

2.1. Materials

Fly ash and waste ash samples were collected from a coal-fired power plant in Wyoming. Fly ash is a lighter form of coal ash that floats into the exhaust stacks. In contrast, bottom ash settles on the ground of the boiler as the heavier component of coal fly ash. Waste ash that is used in this

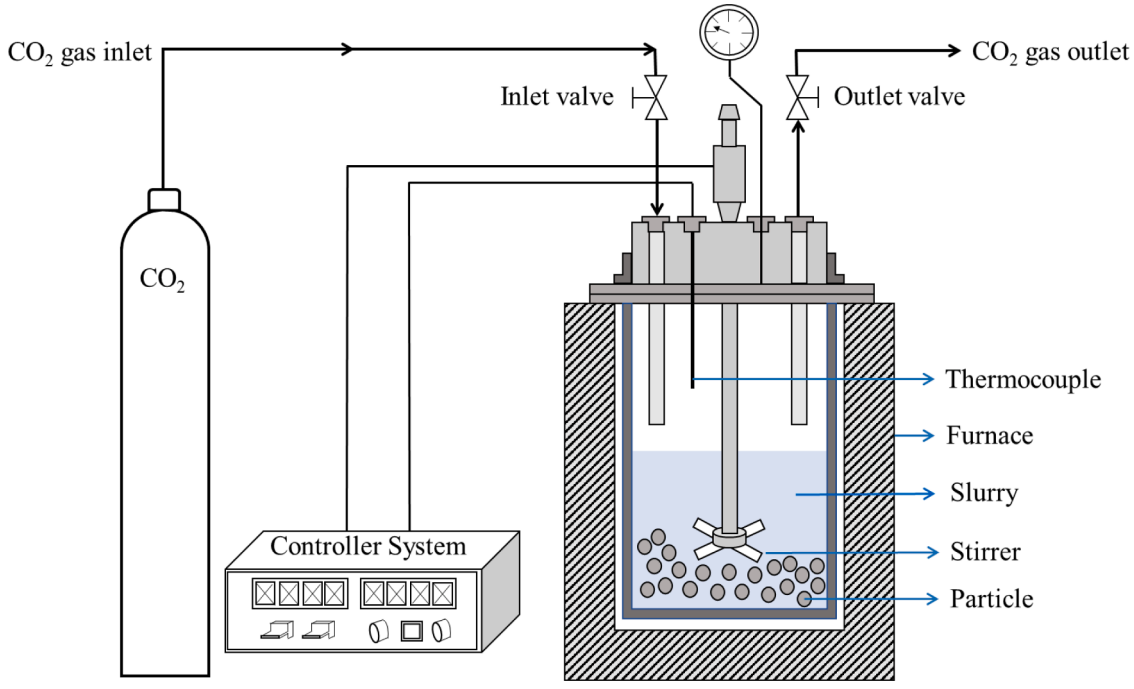

Fig. 2. Schematic representation of the reactor system for continuous CO_2 capture and carbon mineralization of fly ash and waste ash materials.

study is a mixture of fly ash and bottom ash. The chemical compositions of the studied samples were determined using X-ray Fluorescence (XRF) analyses. The major constituent of fly ash and waste ash is calcium oxide (CaO), while minor constituents include magnesium oxide (MgO), iron (III) oxide (Fe_2O_3), and alumina (Al_2O_3) (Table 1). Higher CaO content aids CO_2 capture and carbon mineralization as discussed in the following section. High purity reagents such as sodium hydroxide (NaOH, Fisher Chemical, Certified ACS), glycine ($NH_2CH_2CO_2H$, Alfa Aesar, 99%), MEA (C_2H_7NO, Fisher Chemical, Laboratory Grade), CTAB ($C_{19}H_{42}NBr$, MP Biomedicals, Molecular Biology Grade), calcium nitrate tetrahydrate ($Ca(NO_3)_2 \bullet 4H_2O$, Sigma-Aldrich, ACS reagent), and CO_2 gas (Airgas, 99.8% purity) are used in this study.

2.2. Integrated CO_2 capture and carbon mineralization with fly ash and waste ash

A series of experiments were conducted using fly ash and waste ash samples to investigate carbon mineralization behavior using regenerable solvents. Experiments were performed at a temperature of 50 C for a reaction time of 3 , 15 wt% solid and CO_2 partial pressure of 1 atm and a stirring rate of 300 rpm (± 5 rpm). 2.5 M sodium glycinate was prepared by dissolving equimolar compositions of sodium hydroxide (NaOH) and glycine powders in an appropriate volume of water. Similarly, 30 wt.% (± 1 wt.%) MEA solution was prepared by mixing 30 ml of MEA and 70 ml of water to produce a homogeneous aqueous solution. Experiments were performed with pure water as the base case.

All ash sample experiments were performed in a stainless-steel stirred reactor (Micro Bench Top Reactor, Parr Instrument Company). Fig. 2 shows a schematic representation of the reactor. First, 3.0 g fly ash or waste ash was placed in the reactor and 17 mL of the liquid solution was added to prepare a slurry with 15 wt.% (± 1 %) solid. The system was purged with CO_2 for 3–5 min to remove gas impurities. The system was then heated, and the gas pressure was set to the desired value. The start of the reaction was marked by reaching the desired temperature setpoint of 50 °C. At the end of the reaction time of 3 h, the reactor system was cooled, and the products were collected. The solids were separated using vacuum filtration and dried in a vacuum oven. The dried samples were further used to characterize the carbonate content and the morphologies of these materials.

2.3. Nano-scale calcium carbonate synthesis using regenerable CO_2 capture solvents and surfactants

In this study, nano-scale calcium carbonate is synthesized using sodium glycinate to capture CO_2 and CTAB to suppress the growth of $CaCO_3$ particles. We use a solution of 1 M calcium nitrate as the source of calcium ions, 3 M CO_2-loaded sodium glycinate, and CTAB concentrations of 0, 0.5, and 1 wt.% to investigate the feasibility of producing calcium carbonate while suppressing the growth of calcium carbonate particles. First, Na-glycinate solution was prepared by dissolving equimolar solution of NaOH and glycine in the appropriate quantity of water. CO_2 was loaded on sodium glycinate by supplying 20 kPa (± 5 kPa) of CO_2 to the Na-glycinate solution. Next, 15 ml of CO_2-loaded Na-glycinate solution was added to 10 mL of 2.5 M $Ca(NO_3)_2$ solution to produce calcium carbonate. After mixing, the solution has 25 mL of 1 M $Ca(NO_3)_2$ and 3 M CO_2-loaded Na-glycinate. The reactions occur at 25 ℃ and atmospheric pressure under a constant stirring rate of 300 rpm (± 5 rpm). After 1 h of reaction, the generated precipitate is separated using vacuum filtration and is dried in an oven at 80 ℃ for at least 12 h for further analyses. For the reaction system with CTAB, 0.5 or 1 wt.% of CTAB was added to 5 M Na-glycinate solution before CO_2 loading. Sodium glycinate captures CO_2 from the gas phase and supplies high concentrations of carbonate ions, which is essential for calcium carbonate formation (Liu et al., 2021; Liu and Gadikota, 2020). CTAB suppresses the particle growth of calcium carbonate particles by binding to the nucleating calcium carbonate surfaces and limiting extensive growth. The reactions involved are shown in Fig. 1.

2.4. Material characterization for carbon mineralization

The chemical compositions of the starting materials were determined using X-ray Fluorescence (XRF). Detailed information about the XRF analysis: samples are crushed and pulverized according to default preparation procedures. Sample preparation entails the formation of a homogenous glass disk by the fusion of the sample and a lithium tetraborate/lithium metaborate mixture. The Loss On Ignition (LOI) is determined separately and gravimetrically at 1000 °C. The prepared disks are analyzed by wavelength dispersion X-ray fluorescence (WD-XRF). The LOI is included in the matrix correction calculations, which are performed by the XRF software. The thermal behavior of the starting materials and their reacted products were determined using a Thermo Gravimetric Analyzer (TGA, Discovery SDT 650, TA instrument). The carbonate content is determined based on the changes in the sample weight upon heating from room temperature to 1000 ℃ or more and at a constant N_2 flow rate. The crystalline phases of the powders and their products were determined using X-ray diffraction (XRD) analysis (X-ray diffractometer, Bruker D8 Advance ECO powder diffractometer) with Cu Kα radiation (40 kV, 25 mA). The samples were scanned over the 2θ range from 20° to 80°. The particle size distributions of the materials were determined using a zeta sizer (Malvern Nano ZS) and a particle size analyzer (Anton Paar). The pore sizes, surface areas, and pore volumes of synthesized particles are determined using N_2 adsorption-desorption isotherms measured at 77 K using the Brunauer−Emmett−Teller technique (BET, Quantachrome Autosorb iQ Analyzer). The particle morphologies before and after reaction were determined using Scanning Electron Microscopy (SEM, LEO 1550 FESEM).

2.5. Extent of carbon mineralization

The determination of the extent of the carbon mineralization is challenged by the heterogeneous compositions of the ash samples (Table 1). The extent of carbon mineralization is calculated by assuming that only calcium (Ca) and magnesium (Mg) components of fly ash react to produce solid carbonates. The pH of the solutions bearing the alkaline industrial residues and solvents is usually higher than 7.5 which limits the dissolution of Ni and Fe and their subsequent reactivity to produce carbonates (Table 2). Thus, the extent of mineral carbonation should be calculated and estimated based on careful determination of the chemical phases as well as reasonable assumptions. In this paper, several factors are considered when assessing the extent of carbon mineralization. First, only calcium (Ca) and magnesium (Mg) elements are considered to react and produce water insoluble Ca- and Mg-carbonates, while other elements such as Fe and Ni are unlikely to dissolve at pH greater than 7.5 and react to produce respective carbonates. Second, non-carbonate Ca and Mg species are considered for carbon mineralization. Dissolution of solid calcium carbonate at pH greater than 7.5 in material systems bearing alkaline industrial residues and solvents is negligible. Third, the weight changes arise from carbonate formation and the dissolution and re-precipitation of other phases is negligible.

Based on above assumptions, the extent of carbon mineralization achieved is defined as the measured amount of CO_2 stored in the samples as solid carbonate relative to the theoretical maximum CO_2 storage capacity, and could be expressed by Eq. (1):

$$Extent = \frac{Measured\ CO_2\ amount\ in\ the\ samples}{Theoretical\ maximum\ CO_2\ storage\ capacity} \times\ 100\% \quad (1)$$

The solid carbonate content is determined using thermogravimetric analyses (TGA). $CaCO_3$ decomposition generally occurs between 550 and 800 ℃ in an N_2 environment (Babou-Kammoe et al., 2012; Karunadasa et al., 2019; Vance et al., 2015). CO_2 composition is determined based on the weight loss caused by the carbonate decomposition. Our analyses revealed that both the unreacted fly ash and waste ash

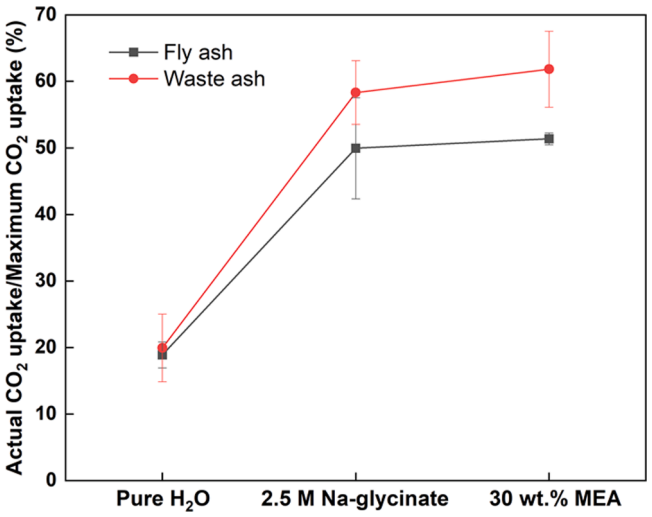

Fig. 3. Actual CO_2 uptake vs. maximum CO_2 uptake in fly ash and waste ash. Experiments were performed at 50 °C for 3 h with 15 wt.% solid in a continuously stirred system and in various solutions as shown.

materials contain around 12 wt% $CaCO_3$.

To determine if the original $CaCO_3$ dissolves during the experiments, the pH values of several solutions before and after reactions are measured (Accumet AE150 pH Benchtop Meter, Fisher Scientific). Solutions bearing sodium glycinate or MEA (with and without CO_2-loading) and the unreacted ash samples had pH levels above 6 which does not favor the dissolution of calcium carbonate present in the unreacted fly ash and waste ash materials.

3. Results and discussion

3.1. Carbon mineralization of fly ash and waste ash

To probe the enhancement in carbon mineralization using regenerable solvents, fly ash and waste ash were reacted in the presence of regenerable CO_2 capture solvents such as 2.5 M sodium glycinate and 30 wt.% mono ethanolamine (MEA). A significant enhancement in the extent of carbon mineralization was noted in the presence of the solvents relative to the base case in which no solvent was used. The extent of non-carbonated calcium converted to calcium carbonate was 18.9% and 19.9%, respectively, when fly ash and waste ash were reacted in only water (Fig. 3). In contrast, the extents of non-carbonate calcium mineralized with fly ash were 49.9% and 51.4% in 2.5 M sodium glycinate and MEA, respectively (Fig. 3). Similarly, the extents of non-carbonate calcium mineralized with waste ash were 58.3% and 61.8% in 2.5 M sodium glycinate and 30 wt.% MEA, respectively (Fig. 3). The content of CaO in fly ash and waste ash are comparable and around 37.4 wt.% and 35.9 wt.%, respectively. The dominant calcium-bearing phases in fly ash and waste ash are calcium oxide, calcium hydroxide, and calcium sulfate (Fig. 4). The higher reactivity of waste ash compared to fly ash is attributed to higher surface area and larger pore volume of waste ash.

Additional insights into the factors underlying the reactivity of waste ash and fly ash are obtained by analyzing the changes in the solution pH and the solubility of the major calcium-bearing constituents of waste ash

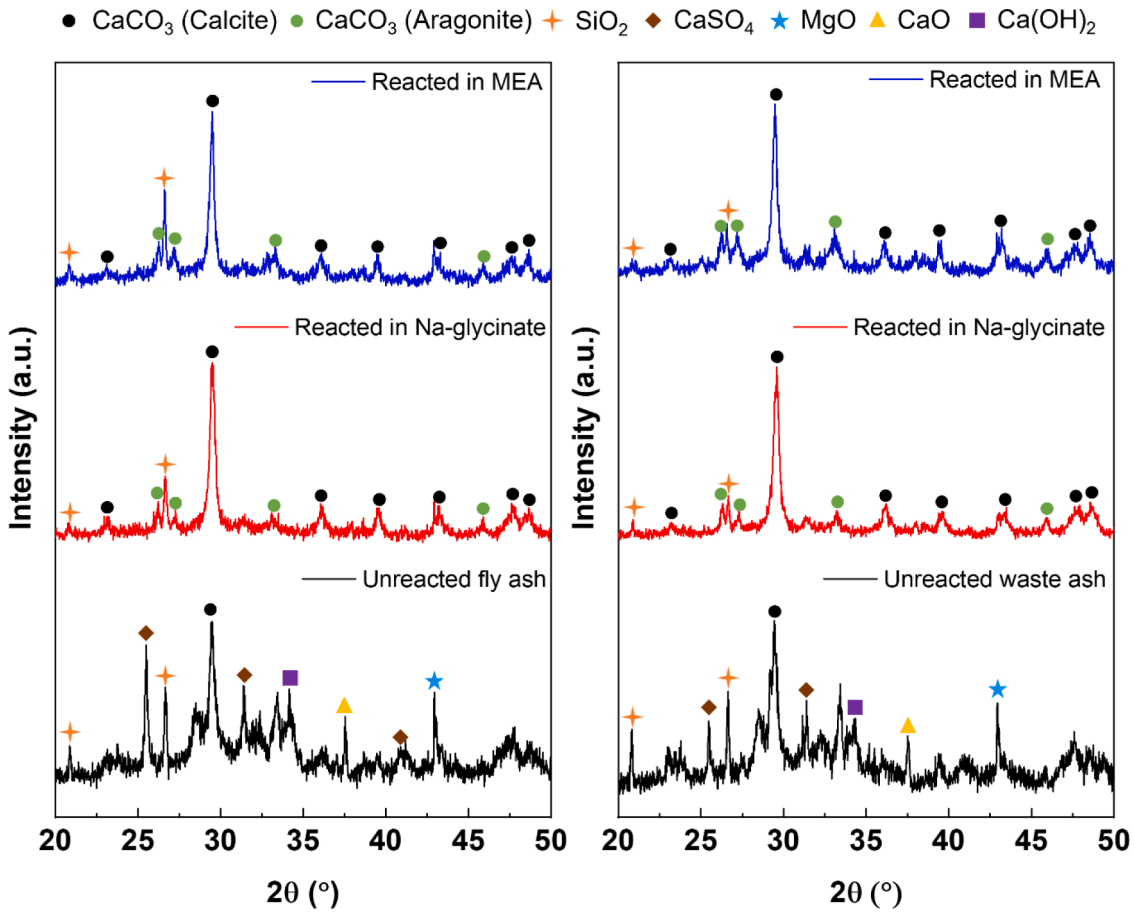

Fig. 4. Evidence of stable calcite and metastable aragonite formation via integrated CO_2 capture and carbon mineralization using MEA and sodium glycinate solvents using X-Ray Diffraction (XRD) analyses.

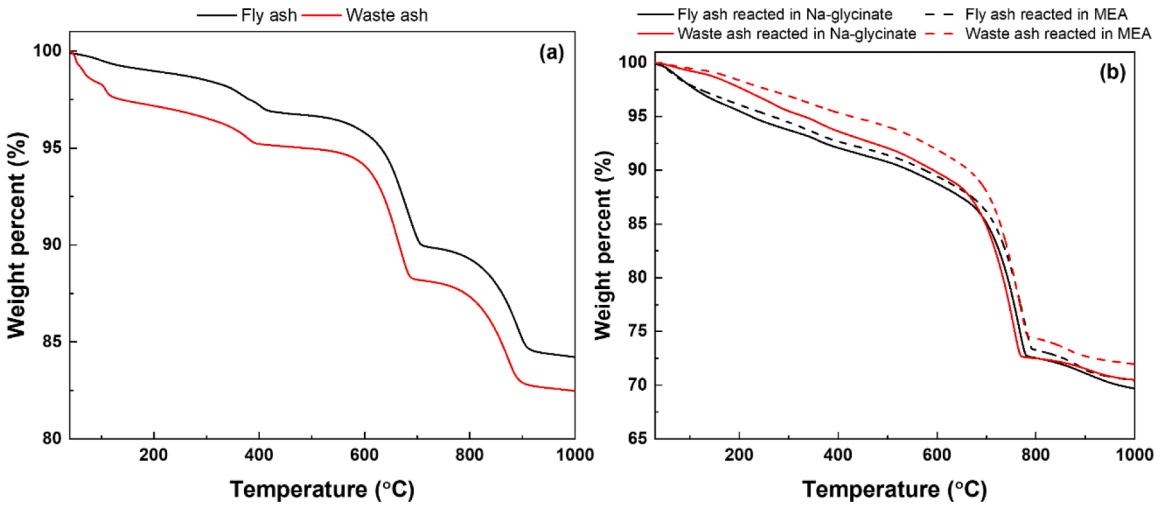

Fig. 5. Evidence of calcium carbonate and calcium hydroxide present in the unreacted fly and waste ash materials (a) and carbonate formation in the reacted fly ash and waste ash materials. The weight loss around 400 °C is attributed to the calcium hydroxide while calcite decomposition is believed to occur around 750 °C–950 °C as shown in the unreacted materials (a). In the reacted products shown in (b), carbonates decomposition is assumed to occur in the range of 550 °C–800 °C. This wide weight loss range results from the mixture of complex alkaline metal carbonates from Ca, Mg and other elements.

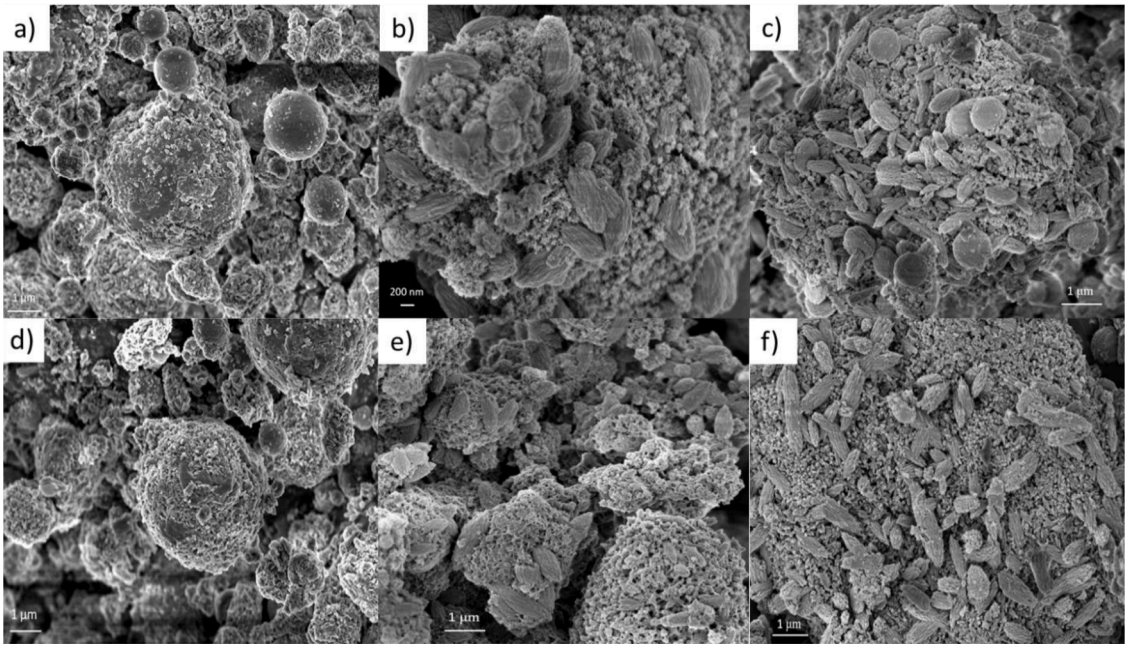

Fig. 6. Evidence of the morphological features of (a) unreacted fly ash, (b) fly ash reacted in sodium glycinate, and (c) fly ash reacted in monoethanolamine (MEA) using SEM images. The morphological features of (d) unreacted waste ash, (e) waste ash reacted in sodium glycinate, and (f) waste ash reacted in monoethanolamine (MEA) are shown.

and fly ash. The solutions obtained after dissolving untreated fly ash and waste ash materials in water at room temperature have a pH greater than 12 which represents the highly alkaline nature of these residues. The solutions that are recovered after reacting these materials in water have pH in the range of 7.1 – 8.7. The solutions recovered after reacting in 2.5 M sodium glycinate and 30 wt.% MEA have pH in the range of 7.9 – 8.2 and 8.3 – 8.6, respectively (Table 2). The feasibility of dissolving the calcium constituents in ash to produce calcium carbonate at these pH conditions can be evaluated based on the solubility behavior of the primary calcium-bearing constituents in the fly ash and waste ash materials.

Insights into the mechanisms underlying carbonate formation are determined based on the relative solubilities of the primary calcium-bearing constituents of fly ash which are calcium oxide, calcium hydroxide, calcium sulfate, and calcium carbonate. Calcium oxide presenting in alkaline industrial residues is readily converted to calcium hydroxide in the presence of water. The solubility products of calcium hydroxide, calcium sulfate, and calcium carbonate are 5.02×10^{-6}, 4.93×10^{-5}, and 3.3×10^{-9}, respectively (Benjamin, 2002; Lide, 2002; Rumble et al., 2018). These data show that the calcium hydroxide and calcium sulfate dissolve preferentially over calcium carbonate, while maintaining all other conditions constant. At pH in the range of 7–9, the solubility of calcium carbonate is significantly lower compared to that of calcium hydroxide and calcium sulfate. Thus, calcium hydroxide (and oxide precursor) and calcium sulfate readily dissolve and precipitate to produce calcium carbonate, while the calcium carbonate present in the original ash materials remains relatively undissolved at these pH conditions. In this study, crystalline calcium silicate phases are not

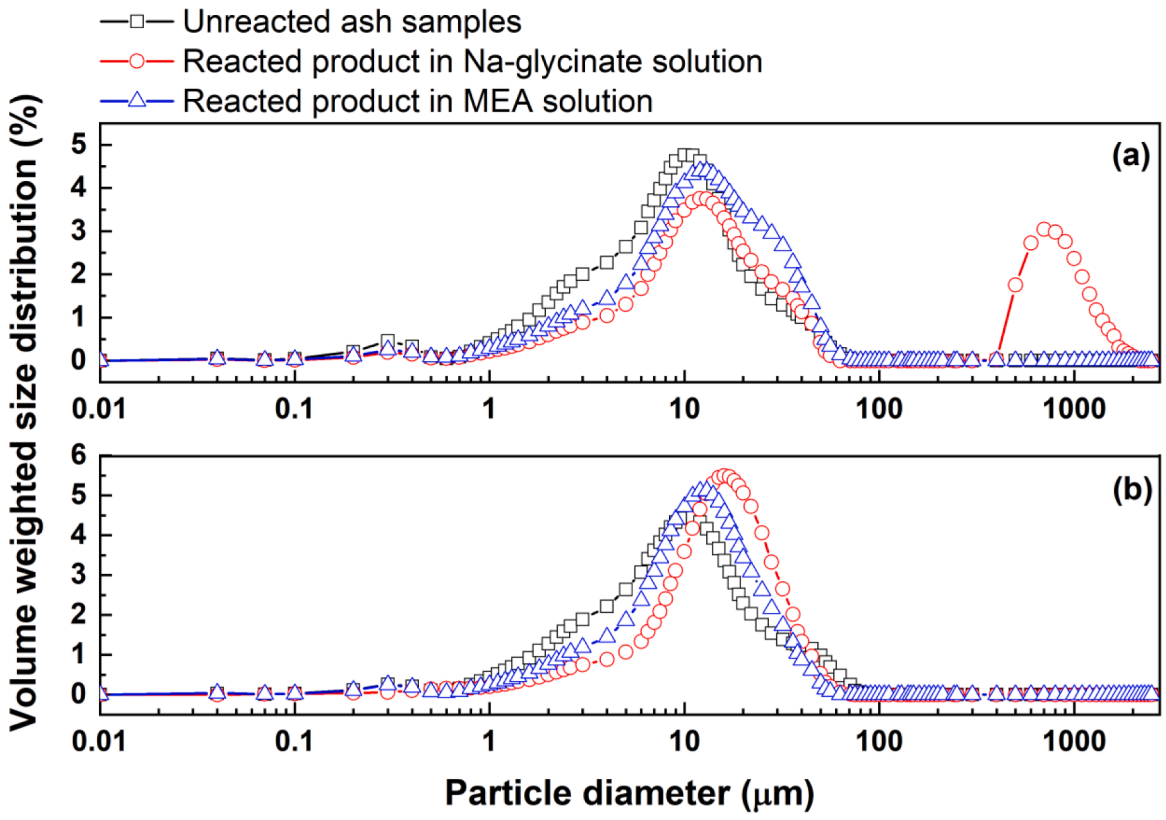

Fig. 7. Particle size distributions of unreacted and reacted (a) fly ash and (b) waste ash materials.

abundant based on the X-Ray Diffraction (XRD) analyses. Prior studies showed that calcium present in silicate phases such as $CaSiO_3$ (wollastonite) reacts with CO_2 to produce calcium carbonate in MEA and sodium glycinate solvents noted in this study. In these scenarios, silica serves as a passivation layer which limits carbon mineralization (Daval et al., 2009b; Gadikota et al., 2020; Kashim et al., 2020; Miller et al., 2013) and only about 35–37% carbonate conversion of pure calcium silicate ($CaSiO_3$) is noted as opposed to near complete conversion of calcium oxide at similar experimental conditions (Liu et al., 2021; Liu and Gadikota, 2020).

The conversion of dominant phases such as calcium oxide, calcium sulfate, and calcium hydroxide to calcium carbonate are evident from detailed X-Ray Diffraction (XRD) analyses when reacted in 2.5 M sodium glycinate or 30 wt.% MEA (Fig. 4). Stable calcite and metastable aragonite phases are dominant in the reacted carbonate-bearing fly ash and waste ash materials (Fig. 4). Moderate temperature (50 °C) and CO_2 pressure (1 atm) contribute to the formation of multiple carbonate phases such as calcite and aragonite. In contrast, higher temperature (200 °C) and pressure (20 bars) favor the formation of stable carbonate phases such as calcite. Minor phases such as Fe_2O_3 are not detected from X-Ray Diffraction (XRD) analyses. No significant changes in the silica (SiO_2) are detected after reactions in fly ash and waste ash samples.

Further evidence of the near complete conversion of calcium hydroxide to calcium carbonate is evident from Thermogravimetric Analysis (TGA). In the unreacted fly ash and waste ash samples, the weight changes in the range of 50–150 °C, 300–480 °C (Liu and Gadikota, 2018), and 750–950 °C correspond to the loss of free water and volatile constituents, decomposition of $Ca(OH)_2$ and the dissociation of $CaCO_3$, respectively. Thus, the weight compositions of free water, $Ca(OH)_2$ and $CaCO_3$ in fly ash are 0.8%, 7%, and 12% and the respective values in waste ash are 2.5%, 6%, and 12% (Fig. 5 **(a)**). Carbon mineralization in the presence of sodium glycinate and mono ethanolamine (MEA) results in near complete conversion of calcium hydroxide to calcium carbonate as noted from the TGA curves, where a single weight loss profile is observed around 750 °C (Fig. 5 **(b)**). This wide decomposition curve is attributed to the existence of mixed metal carbonates.

Extensive carbon mineralization contributes to significant differences in the particle morphology after carbon mineralization of fly ash and waste ash samples as noted from Scanning Electron Microscopy (SEM) images (Fig. 6). The unreacted fly ash and waste ash samples exhibit spherical particle morphologies with sizes ranging from as small as 1–5 μm to larger sizes of 20–30 μm. These observations are consistent with the particle morphologies of fly ash and waste ash materials reported in literature (Heineck et al., 2010; Kutchko and Kim, 2006; Ma et al., 2021). Interestingly, the spheres are attached to each other to form a linked matrix (Fig. 6 **(a) and (d)**). The extensive spherical morphology of fly ash and waste ash materials is reduced upon carbon mineralization and oval-shaped particles are noted. Closer investigation of the oval-shaped particles reveals the formation of rod-like aragonite particles noted in prior studies (Yu et al., 2017). These studies confirm the formation of aragonite particles which is consistent with our observations from XRD analyses (Fig. 4).

The formation of larger particles due to the carbon mineralization of fly ash and waste ash is confirmed using particle size analyses. The unreacted fly ash and waste ash samples have similar particle size distributions in the range of 1–100 μm (Fig. 7). The average particle diameter of the unreacted fly ash and waste ash are 10.96 and 12.35 μm. Carbon mineralization of fly ash and waste ash in the presence of MEA and sodium glycinate results in an increase in the average particle size which is attributed to the growth of newly formed calcium carbonate. A small decrease in the particle size of the fly ash and waste ash materials in the range of 1–10 μm is attributed to the dissolution of the ash particles. The mean particle diameters of the fly ash and waste ash materials reacted in MEA are 14.56 μm and 12.72 μm, respectively. Similarly, the mean particle diameters of the fly ash and waste ash materials reacted in sodium glycinate are 261.90 μm and 16.08 μm, respectively. The mean diameter is not the only parameter representative of the changes in the particle size distribution since multi-modal particle size distributions

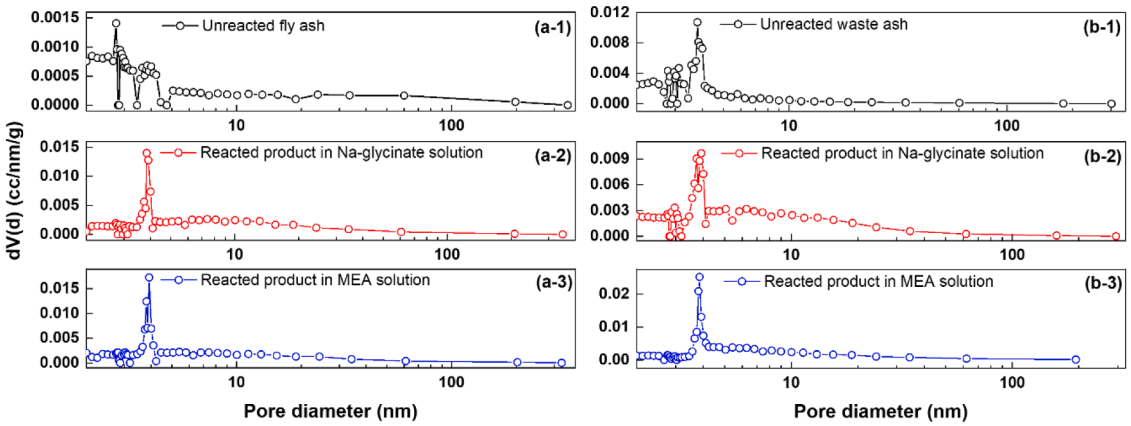

Fig. 8. Pore size distributions for **(a-1)** unreacted and (**a-2** and **a-3**) reacted fly ash and **(b-1)** unreacted and (**b-2** and **b-3**) reacted waste ash materials determined using BET measurements.

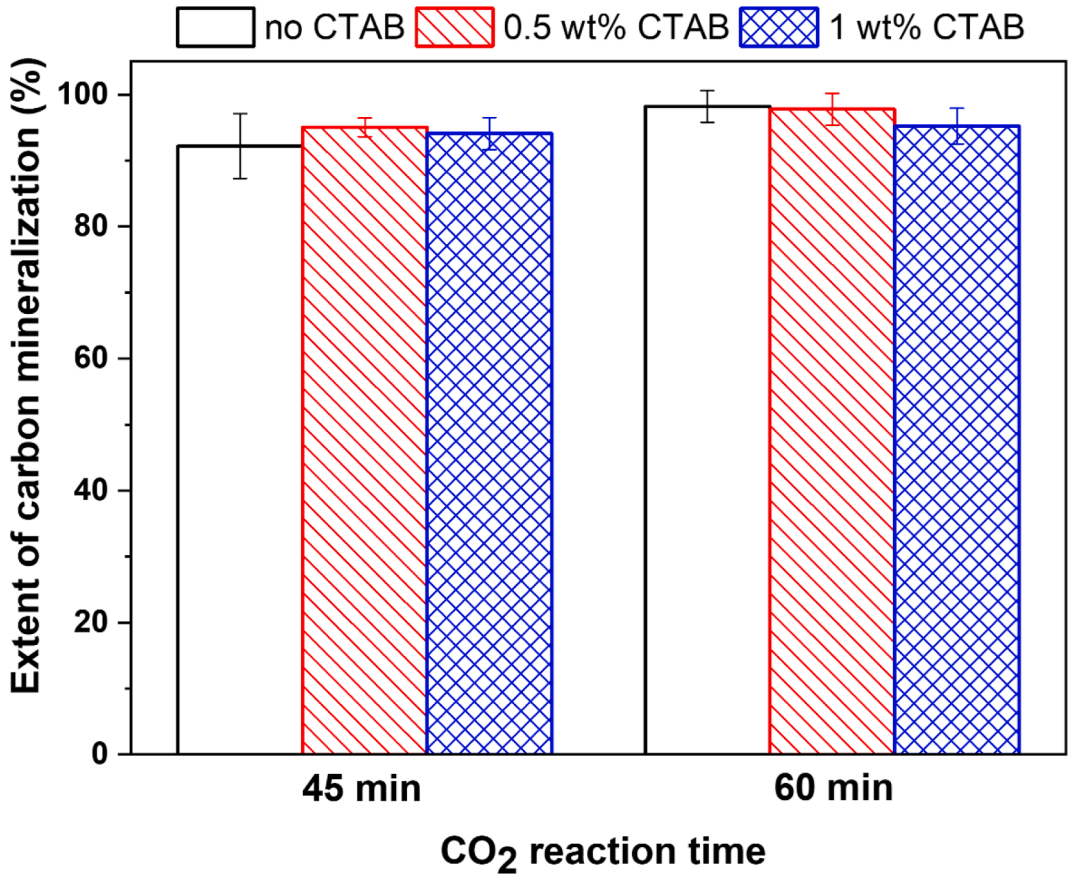

Fig. 9. Extent of calcium carbonate formation from calcium nitrate solutions in the presence and absence of CTAB surfactants.

emerge on carbon mineralization (Fig. 7 **(a) red line**).

This trend in the dissolution of small particles smaller than 10 μm and the associated peak shift to larger particle diameters or increase in the intensity of particles of 20 – 30 μm due to carbonate formation is consistent with prior studies reporting direct carbon mineralization of magnesium-bearing silicate ($(Mg,Fe)_2SiO_4$, olivine) to produce magnesium carbonate (Gadikota et al., 2020, Gadikota et al., 2014). Insights from the particle size analyses (Fig. 7) and SEM images (Fig. 6) show that the newly formed calcium carbonate phases precipitate on the surface of the existing particles as opposed to forming discrete particle size distributions.

The competing effects of the dissolution of alkaline industrial residues and minerals on increasing the pore size and surface area and that of carbonate formation in closing the pore spaces and reducing the pore volume are investigated. The changes in the surface area and pore morphology of the unreacted and reacted fly ash and waste ash materials are determined using Brunauer-Emmett-Teller surface (BET) method using N_2 adsorption approach. The average pore size, surface area and cumulative pore volume of the unreacted and reacted fly ash and waste ash materials are summarized in Table 3.

A significant increase in the surface area and pore volume of the reacted fly ash and waste ash materials are noted on carbon mineralization in the presence of MEA and sodium glycinate. The surface area of the fly ash reacted in MEA and sodium glycinate is 26 m^2/g compared to

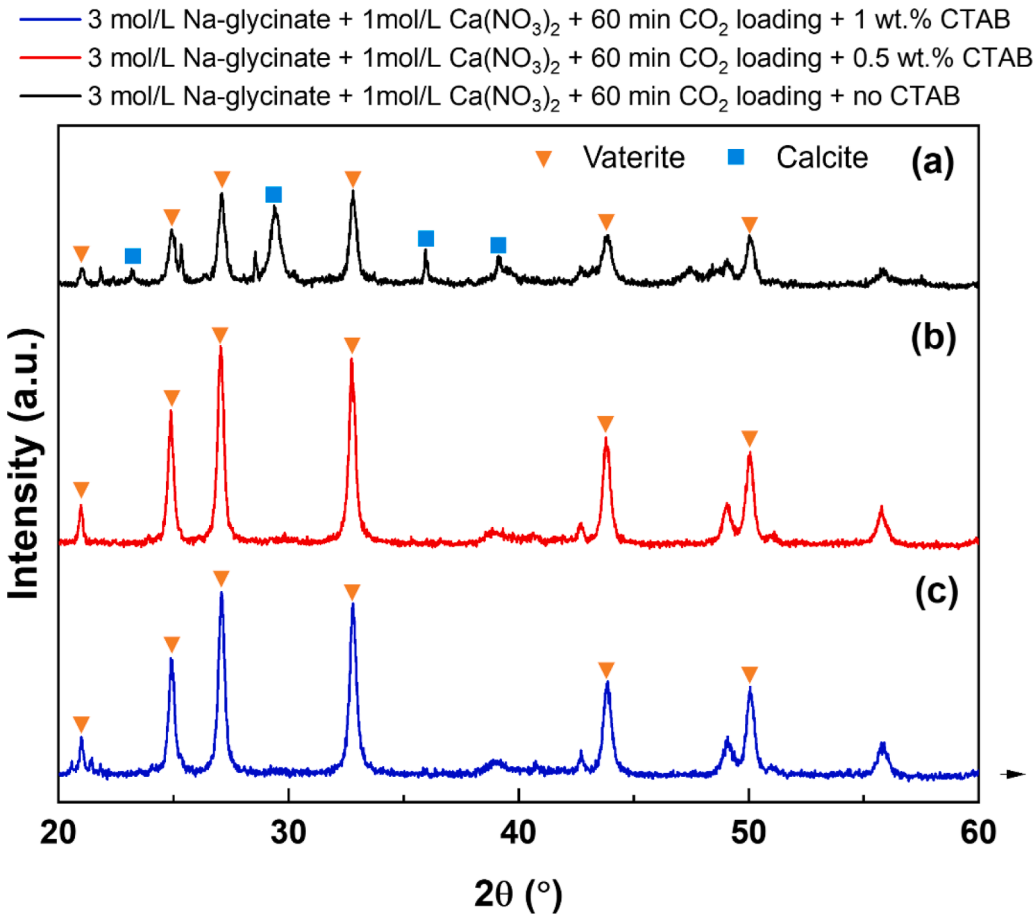

Fig. 10. Effect of CTAB addition on the formation of calcium carbonate phases where (a), (b), and (c) correspond to scenarios with 0, 0.5, and 1 wt% CTAB, respectively using Wide Angle X-Ray Scattering (WAXS) measurements.

Table 2
pH of the solutions recovered after the reaction of fly ash and waste ash with CO_2 to produce calcium carbonate. The pH of the untreated fly ash and waste ash when dissolved in water is greater than 12 which is indicative of the high alkaline content in these materials.

	Fly ash	Waste ash
Solutions obtained after reacting in H_2O	7.56–8.68	7.15–7.33
Solutions obtained after reacting in 2.5 M Na-glycinate	7.93–8.21	8.10–8.15
Solutions obtained after reacting in 30 wt.% MEA	8.46–8.62	8.29–8.38

Table 3
Comparison of the surface area, pore volume, and pore diameter of unreacted and reacted fly ash and waste ash materials.

Sample ID	Surface Area (m^2/g)	Pore Volume (cc/g)	Pore Diameter (nm)
Unreacted fly ash	5.05	0.028	2.75
Fly ash reacted in Na-glycinate	26.07	0.102	3.84
Fly ash reacted in MEA	26.13	0.101	3.91
Waste ash	16.20	0.034	3.80
Waste ash reacted in Na-glycinate	30.60	0.084	3.91
Waste ash reacted in MEA	31.28	0.108	3.85

the unreacted fly ash which is 5 m^2/g. Similarly, the surface area of the waste ash reacted in MEA and sodium glycinate is 31 m^2/g while that of the unreacted precursor is 16 m^2/g. These data suggest that the simultaneous and localized dissolution and carbonate formation in fly ash and waste ash contributes to an increase in the surface area. Furthermore, the cumulative pore volume of fly ash and waste ash materials is a factor of 2.5 – 3.6 higher compared to the unreacted materials. Similarly, an increase in the pore diameter is noted when fly ash and waste ash are reacted in MEA and sodium glycinate.

Further insights into the changes in the pore morphology are obtained by analyzing the pore volume distributions. The unreacted fly ash and waste ash materials have broad pore size distributions in the range of 2.7–5 nm. However, carbon mineralization results in a uniform and narrower pore distribution in the range of 3.5–4.2 nm (Fig. 8) in the reacted fly ash and waste ash materials. These observations are consistent with prior studies that showed the evolution of well-defined pore size distributions on extensive carbon mineralization of magnesium silicate minerals ($(Mg, Fe)_2SiO_4$, olivine). Thus, the competing effects of the dissolution of calcium hydroxide and calcium sulfate and formation of newly formed calcium carbonate contribute to increases in the surface area, pore volume and pore diameter and the formation of well-defined pore volume distributions.

3.2. Nano-scale calcium carbonate synthesis using CO_2 capture solvent (e.g., sodium glycinate) and surfactant (e.g., CTAB)

The ability to synthesize nano-scale calcium carbonate directly using CO_2 in the gas phase unlocks the potential for CO_2 capture and utilization using calcium-rich alkaline residues. Advances in electrodialysis (Kumar et al., 2019) now enable us to produce acids and bases directly from brine. These electrochemically produced acids can be used to dissolve Ca-rich residues such as fly ash or waste ash and produce

Table 4
Average particle sizes of calcium carbonate ($CaCO_3$) obtained with and without the addition of CTAB.

$Ca(NO_3)_2$	CTAB	Na-glycinate	CO_2 loading time	Average size Diameter ≤ 300 nm	Standard deviation	Average size 300 nm < Diameter	Standard deviation
1 M	0 wt.%	3 M	60 min	N/A	N/A	691.10 nm	130.20 nm
1 M	0.5 wt.%	3 M	60 min	184.16 nm	52.87 nm	531.59 nm	179.33 nm
1 M	1 wt.%	3 M	60 min	197.01 nm	61.76 nm	659.21 nm	191.35 nm

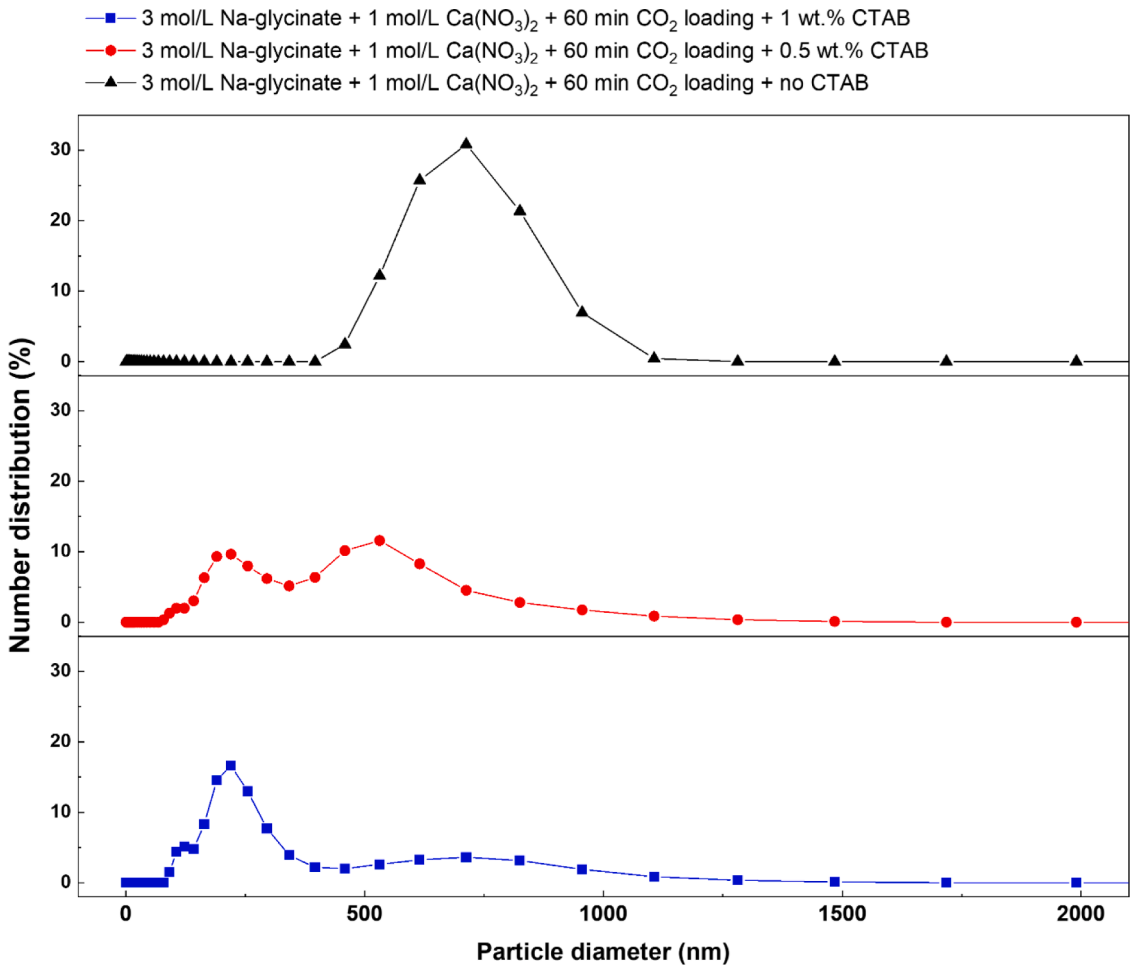

Fig. 11. Effect of CTAB addition on the particle size distributions of the precipitated calcium carbonate where (a), (b), and (c) correspond to scenarios with 0, 0.5, and 1 wt% CTAB, respectively.

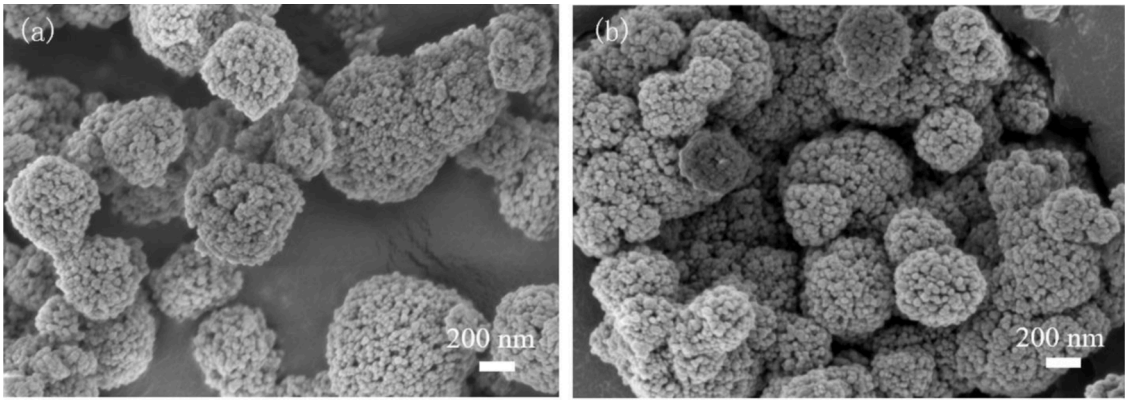

Fig. 12. Evidence of the changes in the morphology of precipitated calcium carbonate (a) without CTAB and (b) 0.5 wt% CTAB. All other conditions such as the concentration of 1 M calcium nitrate, 3 M sodium glycinate, and with continuous CO_2 loading are held constant.

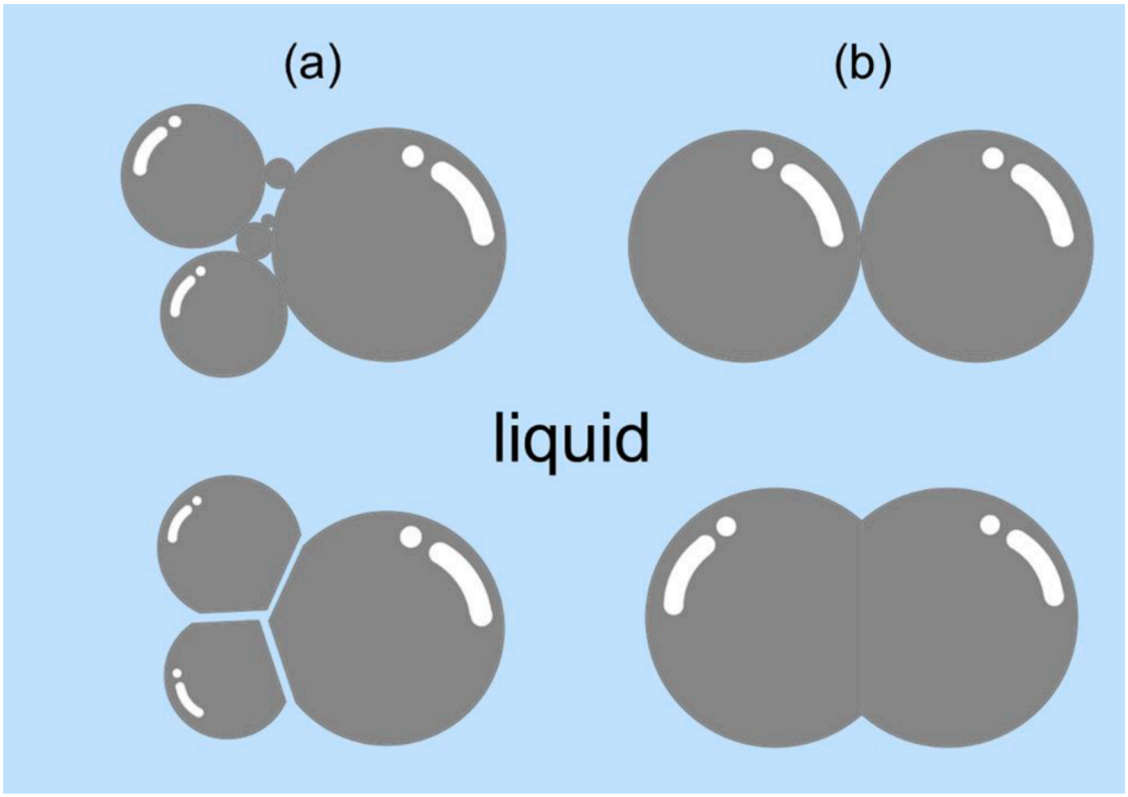

Fig. 13. Suggested mechanisms associated with calcium carbonate growth where (a) and (b) represent Ostwald-Ripening and solid-state bonding, respectively.

calcium-rich solutions for carbon mineralization. High purity calcium-bearing solutions are recovered based on ion separations. These recovered calcium-rich solutions are used to precipitate nano-scale calcium carbonate using anthropogenic CO_2.

Our results showed that more than 90% conversion of dissolved calcium nitrate solution to calcium carbonate particles is achieved on reacting for 45 and 60 min. On reacting for 45 min, the extents of carbonate formation without CTAB, with 0.5 wt.% CTAB and with 1.0 wt.% CTAB are 92.2%, 95.1%, and 94.1%, respectively. Slightly higher extents of carbon mineralization of 98.2%, 97.7% and 95.2% are noted when the reaction time is 60 min in cases without CTAB, with 0.5 wt.% CTAB and with 1 wt.% CTAB, respectively (Fig. 9). The estimated error is in the range of 4-5%. These results show that the addition of CTAB did not have a significant effect on enhancing carbonate formation (Fig. 9).

The hypothesis that surfactants such as CTAB influence the phases of calcium carbonate formed is investigated by analyzing the X-ray diffraction patterns of the calcium carbonate end-product with and without the addition of CTAB. These analyses showed that metastable vaterite and stable calcite phases are co-present when CTAB is not used. This observation is consistent with the formation of stable and metastable calcium carbonate phases when sodium glycinate is used for CO_2 capture and mineralization of calcium oxide (Liu and Gadikota, 2020). The presence of multiple carbonate phases is also in agreement with the previous result when MSWI-bottom ash was utilized as the starting material (Höllen et al., 2018). However, the addition of CTAB leads to the formation of metastable vaterite, whereas stable calcite phases are not observed (Fig. 10). We hypothesize that this vaterite-calcite phase transformation is related to the presence of CTAB. In these experiments, calcium carbonate initially precipitates as vaterite. CTAB binds to the vaterite particles and prevents transformation to a more stable calcium carbonate phase such as calcite. In the absence of CTAB, transformations of vaterite to calcite are favored.

Particle size analyses of calcium carbonate product showed that the average particle diameter of precipitated calcium carbonate is 691.1 nm in the absence of CTAB. However, the addition of 0.5 wt.% CTAB results in a bimodal distribution with mean particle sizes of 184.2 nm and 531.6 nm, respectively. Similarly, the addition of 1 wt.% CTAB results in bimodal distributions with mean particle sizes of 197.0 nm and 659.2 nm, respectively (Table 4 and Fig. 11). At a higher CTAB concentration of 1 wt.%, the peak intensity around 600 nm is significantly lower compared to the CTAB concentration at 0.5 wt.%. These results reveal that higher CTAB concentrations are effective in suppressing the growth of calcium carbonate particles. These observations are corroborated with SEM images.

The effect of CTAB on the morphology of $CaCO_3$ particles is evident from SEM images shown in Fig. 11. Spherical aggregates with smaller nano-scale particles are noted. These smaller nano-scale particles have a vaterite structure which is spherical in shape (Gadikota et al., 2015; Pouget et al., 2010; Trushina et al., 2014). Fig. 11 **(a) and (b)** represents the morphology of calcium carbonate particles without and with 0.5 wt.% CTAB. In the absence of CTAB, most of the particles have a particle diameter larger than 400 nm (Fig. 11 **(a)**). However, the addition of CTAB results in particles that are smaller in size (Fig. 11 **(b)**).

When considering the mechanisms underlying calcium carbonate formation, it is essential to consider surface energy associated with producing particles of varying sizes. Because surface energy of larger particles is lower when compared to small particles, larger particles are more stable and more likely to be generated (Song et al., 2020). The addition of surfactants such as CTAB alters the surface zeta potential since it can neutralize the negative surface charge developed at the $CaCO_3$ surface (El-Sheikh et al., 2013). There are two possible particle growth mechanisms that can lead to the disappearance of small particles. The first mechanism for particle growth is called Ostwald Ripening (Song et al., 2020), which is shown in Fig. 13 **(a)**. In Ostwald Ripening, small solid particles decompose, and the associated solute diffuses through the liquid and re-precipitates on larger particles which leads to the growth of large particles and the disappearance of small particles (Huo et al., 2010).

In Fig. 13 **(b)**, a peanut-shaped particle, formed by the aggregation of two spherical particles, can be observed. Formation of this peanut-like particle can be attributed to another possible particle growth mechanism called solid-state bonding (Yu et al., 2005), which is illustrated in Fig. 13 **(b)**. When two particles have an inter-particle contact surface, based on the solid-state bonding theory, the inter-particle contact area enlarges gradually. Meanwhile, nanoparticles in the two aggregated micro particles redistribute along the liquid wetted particle boundary, forming the peanut-shaped particles (Huo et al., 2010). The peanut-shaped particle morphologies are evident with and without CTAB (Fig. 12). However, smaller particle sizes are noted in the presence of CTAB due to the adsorption of these molecules on the surface of $CaCO_3$ particles which limits crystal growth, dissolution of small particles, and inter-particle contact (Barhoum et al., 2014; El-Sheikh et al., 2013).

4. Conclusions

Accelerated low temperature integrated CO_2 capture and carbon mineralization of fly ash and waste ash is realized using regenerable solvents such as sodium glycinate and monoethanolamine which increase the concentration of dissolved bicarbonate and carbonate species in the aqueous phase and favor carbon mineralization. Fly ash and waste ash conversions of calcium and magnesium to produce carbonates in the range of 50%–60% are achieved at 50 ℃, CO_2 pressure of 1 atm, reaction time of 3 h and in well-stirred environments. The co-presence of calcite and aragonite is noted in the reacted materials. An increase in the particle size, pore volume and surface area in the final products is noted on carbon mineralization.

Furthermore, the role of regenerable CO_2 capture solvents in enabling the synthesis of high purity nanoscale calcium carbonate is investigated. The synergistic combination of sodium glycinate and CTAB which increase the concentration of carbonate species in the aqueous phase and direct the formation of nanoscale calcium carbonate, respectively are noted. The addition of CTAB significantly suppresses the growth of larger calcium carbonate particles by binding to the nucleated calcium carbonate particles and preventing further growth. These studies demonstrate that low-cost CO_2 capture solvents can be used in regenerable CO_2 capture and carbon mineralization cycles from heterogeneous alkaline industrial waste precursors such as fly ash and waste ash.

CRediT authorship contribution statement

Tianhe Yin: Methodology, Formal analysis, Writing – original draft. **Shufan Yin:** Methodology, Formal analysis, Writing – original draft. **Akanksha Srivastava:** Methodology, Formal analysis. **Greeshma Gadikota:** Conceptualization, Methodology, Formal analysis, Writing – review & editing.

Declaration of Competing Interest

The authors declare that they have no known competing financial interests or personal relationships that could have appeared to influence the work reported in this paper.

Acknowldgments

The authors gratefully acknowledge the Cornell Atkinson Academic Venture Fund for supporting these studies. The authors also acknowledge the use of the shared facilities at the Cornell Center for Materials Research (CCMR) which are supported through the National Science Foundation Materials Research Science and Engineering Centers (NSF MRSEC) program (DMR-1719875) and the Cornell Energy Systems Institute (CESI). G. G.'s contributions are supported by the DOE Advanced Manufacturing Office DE-EE0009391. A. S.'s efforts are supported by the Cornell Engineering Learning Initiative which supports research activities for undergraduate students.

References

Azdarpour, A., Asadullah, M., Junin, R., Manan, M., Hamidi, H., Daud, A.R.M., 2014. Carbon dioxide mineral carbonation through pH-swing process: a review. Energy Procedia 61, 2783–2786. https://doi.org/10.1016/j.egypro.2014.12.311.

Azdarpour, A., Asadullah, M., Mohammadian, E., Hamidi, H., Junin, R., Karaei, M.A., 2015. A review on carbon dioxide mineral carbonation through pH-swing process. Chem. Eng. J. 279, 615–630. https://doi.org/10.1016/j.cej.2015.05.064.

Babiker, D., and Ahlstrand, M., 2019. Experimental study of mineral carbonation of wollastonite for increased CO_2 uptake, Thesis, KTH, School of Architecture and the Built Environment.

Babou-Kammoe, R., Hamoudi, S., Larachi, F., Belkacemi, K., 2012. Synthesis of $CaCO_3$ nanoparticles by controlled precipitation of saturated carbonate and calcium nitrate aqueous solutions. Can. J. Chem. Eng. 90, 26–33. https://doi.org/10.1002/cjce.20673.

Baciocchi, R., Costa, G., Polettini, A., Pomi, R., 2009. Influence of particle size on the carbonation of stainless steel slag for CO_2 storage. Energy Procedia 1, 4859–4866. https://doi.org/10.1016/j.egypro.2009.02.314.

Barhoum, A., Rahier, H., Abou-Zaied, R.E., Rehan, M., Dufour, T., Hill, G., Dufresne, A., 2014. Effect of cationic and anionic surfactants on the application of calcium carbonate nanoparticles in paper coating. ACS Appl. Mater. Interfaces 6, 2734–2744. https://doi.org/10.1021/am405278j.

Bauer, M., Gassen, N., Stanjek, H., Peiffer, S., 2011. Carbonation of lignite fly ash at ambient T and P in a semi-dry reaction system for CO_2 sequestration. Appl. Geochem. 26, 1502–1512. https://doi.org/10.1016/j.apgeochem.2011.05.024.

Benhelal, E., Hook, J.M., Rashid, M.I., Zhao, G., Oliver, T.K., Rayson, M.S., Brent, G.F., Stockenhuber, M., Kennedy, E.M., 2021. Insights into chemical stability of Mg-silicates and silica in aqueous systems using ^{25}Mg and ^{29}Si solid-state MAS NMR spectroscopy: applications for CO_2 capture and utilisation. Chem. Eng. J. 420, 127656 https://doi.org/10.1016/j.cej.2020.127656.

Benjamin, M.M., 2002. Water Chemistry, McGraw-Hill Series in Water Resources and Environmental Engineering. McGraw-Hill.

Bobicki, E.R., Liu, Q., Xu, Z., 2014. Ligand-promoted dissolution of serpentine in ultramafic nickel ores. Miner. Eng. 64, 109–119. https://doi.org/10.1016/j.mineng.2014.05.020.

Bonenfant, D., Kharoune, L., Sauvé, S., Hausler, R., Niquette, P., Mimeault, M., Kharoune, M., 2008. CO_2 sequestration potential of steel slags at ambient pressure and temperature. Ind. Eng. Chem. Res. 47, 7610–7616. https://doi.org/10.1021/ie701721j.

Chang, E.E., Chen, C.H., Chen, Y.H., Pan, S.Y., Chiang, P.C., 2011a. Performance evaluation for carbonation of steel-making slags in a slurry reactor. J. Hazard. Mater. 186, 558–564. https://doi.org/10.1016/j.jhazmat.2010.11.038.

Chang, E.E., Pan, S.Y., Chen, Y.H., Chu, H.W., Wang, C.F., Chiang, P.C., 2011b. CO_2 sequestration by carbonation of steelmaking slags in an autoclave reactor. J. Hazard. Mater. 195, 107–114. https://doi.org/10.1016/j.jhazmat.2011.08.006.

Chang, E.E., Pan, S.Y., Chen, Y.H., Tan, C.S., Chiang, P.C., 2012. Accelerated carbonation of steelmaking slags in a high-gravity rotating packed bed. J. Hazard. Mater 227–228, 97–106. https://doi.org/10.1016/j.jhazmat.2012.05.021.

Chen, H., Wang, F., Zhao, C., Duan, L., 2018. Carbonation kinetics of fly-ash-modified calcium-based sorbents for CO_2 capture. Greenh. Gases Sci. Technol. 8, 292–308. https://doi.org/10.1002/ghg.1739.

Daval, D., Martinez, I., Corvisier, J., Findling, N., Goffé, B., Guyot, F., 2009a. Carbonation of Ca-bearing silicates, the case of wollastonite: experimental investigations and kinetic modeling. Chem. Geol. 265, 63–78. https://doi.org/10.1016/j.chemgeo.2009.01.022.

Daval, D., Martinez, I., Guigner, J.M., Hellmann, R., Corvisier, J., Findling, N., Dominici, C., Goffé, B., Guyot, F., 2009b. Mechanism of wollastonite carbonation deduced from micro- to nanometer length scale observations. Am. Mineral. 94, 1707–1726. https://doi.org/10.2138/am.2009.3294.

Declercq, J., Bosc, O., Oelkers, E.H., 2013. Do organic ligands affect forsterite dissolution rates? Appl. Geochem. 39, 69–77. https://doi.org/10.1016/j.apgeochem.2013.09.020.

Di Lorenzo, F., Ruiz-Agudo, C., Ibañez-Velasco, A., Gil-San Millán, R., Navarro, J.A.R., Ruiz-Agudo, E., Rodriguez-Navarro, C., 2018. The carbonation of wollastonite: a model reaction to test natural and biomimetic catalysts for enhanced CO_2 sequestration. Minerals 8. https://doi.org/10.3390/min8050209.

Ding, W., Fu, L., Ouyang, J., Yang, H., 2014. CO_2 mineral sequestration by wollastonite carbonation. Phys. Chem. Miner. 41, 489–496. https://doi.org/10.1007/s00269-014-0659-z.

Donnet, M., Bowen, P., Jongen, N., Lemaître, J., Hofmann, H., 2005. Use of seeds to control precipitation of calcium carbonate and determination of seed nature. Langmuir 21, 100–108. https://doi.org/10.1021/la048525i.

El-Sheikh, S.M., El-Sherbiny, S., Barhoum, A., Deng, Y., 2013. Effects of cationic surfactant during the precipitation of calcium carbonate nano-particles on their size, morphology, and other characteristics. Colloids Surf. A Physicochem. Eng. Asp. 422, 44–49. https://doi.org/10.1016/j.colsurfa.2013.01.020.

Eloneva, S., Teir, S., Salminen, J., Fogelholm, C.J., Zevenhoven, R., 2008. Fixation of CO_2 by carbonating calcium derived from blast furnace slag. Energy 33, 1461–1467. https://doi.org/10.1016/j.energy.2008.05.003.

Gadikota, G., Fricker, K., Jang, S.H., Park, A.H.A., 2015. Carbonation of silicate minerals and industrial wastes and their potential use as sustainable construction materials 295–322. 10.1021/bk-2015-1194.ch012.

Gadikota, G., Matter, J., Kelemen, P., Brady, P.V., Park, A.H.A., 2020. Elucidating the differences in the carbon mineralization behaviors of calcium and magnesium bearing alumino-silicates and magnesium silicates for CO_2 storage. Fuel 277, 117900. https://doi.org/10.1016/j.fuel.2020.117900.

Gadikota, G., Matter, J., Kelemen, P., Park, A.H.A., 2014. Chemical and morphological changes during olivine carbonation for CO_2 storage in the presence of NaCl and $NaHCO_3$. Phys. Chem. Chem. Phys. 16, 4679–4693. https://doi.org/10.1039/c3cp54903h.

Gerdemann, S., Dahlin, D., Oconnor, W., 2003. Carbon dioxide sequestration by aqueous mineral carbonation of magnesium silicate minerals. In: Proceedings of the Greenhouse Gas Control Technologies - 6th International Conference, 677–682. https://doi.org/10.1016/b978-008044276-1/50108-2.

Gollakota, A.R.K., Volli, V., Shu, C.M., 2019. Progressive utilisation prospects of coal fly ash: a review. Sci. Total Environ. 672, 951–989. https://doi.org/10.1016/j.scitotenv.2019.03.337.

Harrison, A.L., Power, I.M., Dipple, G.M., 2013. Accelerated carbonation of brucite in mine tailings for carbon sequestration. Environ. Sci. Technol. 47, 126–134. https://doi.org/10.1021/es3012854.

Heineck, K.S., Lemos, R.G., Flores, J.A.A., Consoli, N.C., 2010. Influence of particle morphology on the hydraulic behavior of coal ash and sand. Geotech. Geol. Eng. 28, 325–335. https://doi.org/10.1007/s10706-009-9294-8.

Höllen, D., Berneder, I., Capo Tous, F., Stöllner, M., Philipp Sedlazeck, K., Schwarz, T., Aldrian, A., Lehner, M., 2018. Stepwise treatment of ashes and slags by dissolution, precipitation of iron phases and carbonate precipitation for production of raw materials for industrial applications. Waste Manag. 78, 750–762. https://doi.org/10.1016/j.wasman.2018.06.048.

Hong, S., Sim, G., Moon, S., Park, Y., 2020. Low-temperature regeneration of amines integrated with production of structure-controlled calcium carbonates for combined CO_2 capture and utilization. Energy Fuels 34, 3532–3539. https://doi.org/10.1021/acs.energyfuels.9b04339.

Huijgen, W.J.J., Witkamp, G.J., Comans, R.N.J., 2006. Mechanisms of aqueous wollastonite carbonation as a possible CO_2 sequestration process. Chem. Eng. Sci. 61, 4242–4251. https://doi.org/10.1016/j.ces.2006.01.048.

Huijgen, W.J.J., Witkamp, G.J., Comans, R.N.J., 2005. Mineral CO_2 sequestration by steel slag carbonation. Environ. Sci. Technol. 39, 9676–9682. https://doi.org/10.1021/es050795f.

Huntzinger, D.N., Gierke, J.S., Sutter, L.L., Kawatra, S.K., Eisele, T.C., 2009. Mineral carbonation for carbon sequestration in cement kiln dust from waste piles. J. Hazard. Mater. 168, 31–37. https://doi.org/10.1016/j.jhazmat.2009.01.122.

Huo, S.H., Qian, M., Schaffer, G.B., Crossin, E., 2010. Aluminium Powder Metallurgy, Fundamentals of Aluminium Metallurgy: Production, Processing and Applications. Woodhead Publishing Limited. https://doi.org/10.1533/9780857090256.3.655.

Ji, L., Yu, H., Zhang, R., French, D., Grigore, M., Yu, B., Wang, X., Yu, J., Zhao, S., 2019. Effects of fly ash properties on carbonation efficiency in CO_2 mineralisation. Fuel Process. Technol. 188, 79–88. https://doi.org/10.1016/j.fuproc.2019.01.015.

Karunadasa, K.S.P., Manoratne, C.H., Pitawala, H.M.T.G.A., Rajapakse, R.M.G., 2019. Thermal decomposition of calcium carbonate (calcite polymorph) as examined by *in-situ* high-temperature X-ray powder diffraction. J. Phys. Chem. Solids 134, 21–28. https://doi.org/10.1016/j.jpcs.2019.05.023.

Kashim, M.Z., Tsegab, H., Rahmani, O., Abu Bakar, Z.A., Aminpour, S.M., 2020. Reaction mechanism of wollastonite *in situ* mineral carbonation for CO_2 sequestration: effects of saline conditions, temperature, and pressure. ACS Omega 2020. https://doi.org/10.1021/acsomega.0c02358.

Kodama, S., Nishimoto, T., Yamamoto, N., Yogo, K., Yamada, K., 2008. Development of a new pH-swing CO_2 mineralization process with a recyclable reaction solution. Energy 33, 776–784. https://doi.org/10.1016/j.energy.2008.01.005.

Korchef, A., Touaibi, M., 2020. Effect of pH and temperature on calcium carbonate precipitation by CO_2 removal from iron-rich water. Water Environ. J. 34, 331–341. https://doi.org/10.1111/wej.12467.

Kumar, A., Phillips, K.R., Thiel, G.P., Schröder, U., Lienhard, J.H., 2019. Direct electrosynthesis of sodium hydroxide and hydrochloric acid from brine streams. Nat. Catal. 2, 106–113. https://doi.org/10.1038/s41929-018-0218-y.

Kutchko, B.G., Kim, A.G., 2006. Fly ash characterization by SEM-EDS. Fuel 85, 2537–2544. https://doi.org/10.1016/j.fuel.2006.05.016.

Lei, M., Li, P.G., Sun, Z.B., Tang, W.H., 2006. Effects of organic additives on the morphology of calcium carbonate particles in the presence of CTAB. Mater. Lett. 60, 1261–1264. https://doi.org/10.1016/j.matlet.2005.11.023.

Li, X., Bertos, M.F., Hills, C.D., Carey, P.J., Simon, S., 2007. Accelerated carbonation of municipal solid waste incineration fly ashes. Waste Manag. 27, 1200–1206. https://doi.org/10.1016/j.wasman.2006.06.011.

Lide, D.R., 2002. CRC Handbook of Chemistry and Physics, 83rd Edition. Taylor & Francis.

Liu, M., Gadikota, G., 2020. Single-step, low temperature and integrated CO_2 capture and conversion using sodium glycinate to produce calcium carbonate. Fuel 275, 117887. https://doi.org/10.1016/j.fuel.2020.117887.

Liu, M., Gadikota, G., 2019. Integrated CO_2 capture, conversion, and storage to produce calcium carbonate using an amine looping strategy. Energy Fuels 33, 1722–1733. https://doi.org/10.1021/acs.energyfuels.8b02803.

Liu, M., Asgar, H., Seifert, S., Gadikota, G., 2020. Novel aqueous amine looping approach for the direct capture, conversion and storage of CO_2 to produce magnesium carbonate. Sustain. Energy Fuels 4 (3), 1265–1275.

Liu, M., Gadikota, G., 2018. Phase evolution and textural changes during the direct conversion and storage of CO_2 to produce calcium carbonate from calcium hydroxide. Geosci 8, 1–2. https://doi.org/10.3390/geosciences8120445.

Liu, M., Hohenshil, A., Gadikota, G., 2021. Integrated CO_2 capture and removal via carbon mineralization with inherent regeneration of aqueous solvents. Energy Fuels 35, 8051–8068. https://doi.org/10.1021/acs.energyfuels.0c04346.

Ma, J., Wang, D., Zhao, S., Duan, P., Yang, S., 2021. Influence of particle morphology of ground fly ash on the fluidity and strength of cement paste. Materials 14, 1–18. https://doi.org/10.3390/ma14020283 (Basel).

Mercer, K.L., Lin, Y.P., Singer, P.C., 2005. Enhancing calcium carbonate precipitation by heterogeneous nucleation during chemical softening. J. Am. Water Work Assoc. 97, 116–125. https://doi.org/10.1002/j.1551-8833.2005.tb07545.x.

Migliardini, F., De Luca, V., Carginale, V., Rossi, M., Corbo, P., Supuran, C.T., Capasso, C., 2014. Biomimetic CO_2 capture using a highly thermostable bacterial α-carbonic anhydrase immobilized on a polyurethane foam. J. Enzyme Inhib. Med. Chem. 29, 146–150. https://doi.org/10.3109/14756366.2012.761608.

Miller, Q.R.S., Thompson, C.J., Loring, J.S., Windisch, C.F., Bowden, M.E., Hoyt, D.W., Hu, J.Z., Arey, B.W., Rosso, K.M., Schaef, H.T., 2013. Insights into silicate carbonation processes in water-bearing supercritical CO_2 fluids. Int. J. Greenh. Gas Control 15, 104–118. https://doi.org/10.1016/j.ijggc.2013.02.005.

Min, Y., Li, Q., Voltolini, M., Kneafsey, T., Jun, Y.S., 2017. Wollastonite carbonation in water-bearing supercritical CO_2: effects of Particle Size. Environ. Sci. Technol. 51, 13044–13053. https://doi.org/10.1021/acs.est.7b04475.

Montes-Hernandez, G., Pérez-López, R., Renard, F., Nieto, J.M., Charlet, L., 2009. Mineral sequestration of CO_2 by aqueous carbonation of coal combustion fly-ash. J. Hazard. Mater. 161, 1347–1354. https://doi.org/10.1016/j.jhazmat.2008.04.104.

Nyambura, M.G., Mugera, G.W., Felicia, P.L., Gathura, N.P., 2011. Carbonation of brine impacted fractionated coal fly ash: Implications for CO_2 sequestration. J. Environ. Manag. 92, 655–664. https://doi.org/10.1016/j.jenvman.2010.10.008.

Pérez-López, R., Montes-Hernandez, G., Nieto, J.M., Renard, F., Charlet, L., 2008. Carbonation of alkaline paper mill waste to reduce CO_2 greenhouse gas emissions into the atmosphere. Appl. Geochem. 23, 2292–2300. https://doi.org/10.1016/j.apgeochem.2008.04.016.

Pouget, E.M., Bomans, P.H.H., Dey, A., Frederik, P.M., De G., Sommerdijk, N.A.J.M., 2010. Vaterite 20, 11560–11565.

Rumble, Lide, David R., Bruno, Thomas J., JR., 2018. CRC handbook of chemistry and physics: a ready-reference book of chemical and physical data.

Russo, M.E., Olivieri, G., Capasso, C., De Luca, V., Marzocchella, A., Salatino, P., Rossi, M., 2013. Kinetic study of a novel thermo-stable α-carbonic anhydrase for biomimetic CO_2 capture. Enzyme Microb. Technol. 53, 271–277. https://doi.org/10.1016/j.enzmictec.2013.05.002.

Sanna, A., Vega, F., Navarrete, B., Maroto-Valer, M.M., 2014. Accelerated MEA degradation study in hybrid CO_2 capture systems. Energy Procedia 63, 745–749. https://doi.org/10.1016/j.egypro.2014.11.082.

Song, X., Zhang, L., Cao, Y., Zhu, J., Luo, X., 2020. Effect of pH and temperatures on the fast precipitation vaterite particle size and polymorph stability without additives by steamed ammonia liquid waste. Powder Technol. 374, 263–273. https://doi.org/10.1016/j.powtec.2020.07.029.

Tai, C.Y., Chen, W.R., Shih, S.M., 2006. Factors affecting wollastonite carbonation under CO_2 supercritical conditions. AIChE J. 52, 292–299. https://doi.org/10.1002/aic.10572.

Anderson, C.P., 2006. Effects of carbonation on the mineral composition of cement kiln dust. M. S. Thesis in Geology, Michigan Technological University.

Trushina, D.B., Bukreeva, T.V., Kovalchuk, M.V., Antipina, M.N., 2014. $CaCO_3$ vaterite microparticles for biomedical and personal care applications. Mater. Sci. Eng. C 45, 644–658. https://doi.org/10.1016/j.msec.2014.04.050.

Uliasz-Bocheńczyk, A., Mokrzycki, E., Piotrowski, Z., Pomykała, R., 2009. Estimation of CO_2 sequestration potential via mineral carbonation in fly ash from lignite combustion in Poland. Energy Procedia 1, 4873–4879. https://doi.org/10.1016/j.egypro.2009.02.316.

Vance, K., Falzone, G., Pignatelli, I., Bauchy, M., Balonis, M., Sant, G., 2015. Direct Carbonation of $Ca(OH)_2$ Using Liquid and Supercritical CO_2: Implications for Carbon-Neutral Cementation. Ind. Eng. Chem. Res. 54, 8908–8918. https://doi.org/10.1021/acs.iecr.5b02356.

Verma, M., Bhaduri, G.A., Phani Kumar, V.S., Deshpande, P.A., 2021. Biomimetic Catalysis of CO_2 Hydration: A Materials Perspective. Ind. Eng. Chem. Res. 60, 4777–4793. https://doi.org/10.1021/acs.iecr.0c06203.

Wang, C., Jia, L., Tan, Y., Anthony, E.J., 2008. Carbonation of fly ash in oxy-fuel CFB combustion. Fuel 87, 1108–1114. https://doi.org/10.1016/j.fuel.2007.06.024.

Wang, F., Dreisinger, D., Jarvis, M., Hitchins, T., 2019. Kinetics and mechanism of mineral carbonation of olivine for CO_2 sequestration. Miner. Eng. 131, 185–197. https://doi.org/10.1016/j.mineng.2018.11.024.

Wang, J., Watanabe, N., Inomoto, K., Kamitakahara, M., Nakamura, K., Komai, T., Tsuchiya, N., 2021. Enhancement of aragonite mineralization with a chelating agent for CO_2 storage and utilization at low to moderate temperatures. Sci. Rep. 11, 1–14. https://doi.org/10.1038/s41598-021-93550-9.

Wang, X., Maroto-Valer, M., 2011. Integration of CO_2 capture and storage based on pH-swing mineral carbonation using recyclable ammonium salts. Energy Procedia 4, 4930–4936. https://doi.org/10.1016/j.egypro.2011.02.462.

Wolff-Boenisch, D., Wenau, S., Gislason, S.R., Oelkers, E.H., 2011. Dissolution of basalts and peridotite in seawater, in the presence of ligands, and CO_2: Implications for mineral sequestration of carbon dioxide. Geochim. Cosmochim. Acta 75, 5510–5525. https://doi.org/10.1016/j.gca.2011.07.004.

Wu, D., 2017. Reuse carbon dioxide emissions via accelerated carbonation. Chem. Eng. Prog. 113, 25.

Xu, B., Yi, Y., 2022. Treatment of ladle furnace slag by carbonation: Carbon dioxide sequestration, heavy metal immobilization, and strength enhancement. Chemosphere 287. https://doi.org/10.1016/j.chemosphere.2021.132274.

Yadav, V.S., Prasad, M., Khan, J., Amritphale, S.S., Singh, M., Raju, C.B., 2010. Sequestration of carbon dioxide (CO_2) using red mud. J. Hazard. Mater. 176, 1044–1050. https://doi.org/10.1016/j.jhazmat.2009.11.146.

Yan, H., Zhang, J., Zhao, Y., Zheng, C., 2013. CO2 Sequestration from flue gas by direct aqueous mineral carbonation of wollastonite. Sci. China Technol. Sci. 56, 2219–2227. https://doi.org/10.1007/s11431-013-5318-y.

Yao, Z.T., Ji, X.S., Sarker, P.K., Tang, J.H., Ge, L.Q., Xia, M.S., Xi, Y.Q., 2015. A comprehensive review on the applications of coal fly ash. Earth-Science Rev 141, 105–121. https://doi.org/10.1016/j.earscirev.2014.11.016.

Yu, B., Yu, H., Li, K., Ji, L., Yang, Q., Chen, Z., Megharaj, M., 2019. Integration of a diamine solvent based absorption and coal fly ash based mineralisation for CO2 sequestration. Fuel Process. Technol. 192, 220–226. https://doi.org/10.1016/j.fuproc.2019.04.030.

Yu, J., Zhao, X., Cheng, B., Zhang, Q., 2005. Controlled synthesis of calcium carbonate in a mixed aqueous solution of PSMA and CTAB. J. Solid State Chem. 178, 861–867. https://doi.org/10.1016/j.jssc.2005.01.002.

Yu, S.H., Li, H., Yao, Q.Z., Fu, S.Q., Zhou, G.T., 2017. Hierarchically nanostructured shuttle-like aragonite mesocrystals: preparation, characterization, growth mechanism, and removal ability to La(III). J. Environ. Chem. Eng. 5, 893–905. https://doi.org/10.1016/j.jece.2017.01.004.